# Experimental test of the optical Bloch equations for solids using free-induction decay

A. Szabo and T. Muramoto*
*Division of Physics, National Research Council of Canada, Ottawa, Ontario, Canada K1A 0R6*
(Received 28 November 1988)

Recent studies by DeVoe and Brewer [Phys. Rev. Lett. **50**, 1269 (1983)] have shown that the conventional optical Bloch equations markedly fail to describe the optical saturation behavior of the $D_1$ line in the solid $Pr^{3+}$:$LaF_3$. In this paper we extend these studies to another solid, ruby, using free-induction-decay observations obtained by pulse excitation of the $R_1$ line at 693.4 nm with an ultranarrow-linewidth dye laser. Comparison of the results with Gauss-Markov and random-telegraph-dephasing theories shows approximate agreement for a fluctuation correlation time $\tau_c = T_2$, the dephasing time. This result is remarkably similar to that obtained for $Pr^{3+}$:$LaF_3$. However, for theoretical and experimental reasons, we conclude that the theories do not consistently explain the current as well as other data. A qualitative discussion of another dephasing model is given.

## I. INTRODUCTION

Recent free-induction-decay (FID) studies by DeVoe and Brewer[1] have shown that the conventional optical Bloch equations (OBE's) fail to describe the saturation behavior of the $D_1$ line (592.5 nm) in $Pr^{3+}$:$LaF_3$. This is a surprising and important result both for scientific and technological reasons. For hole-burning optical memories[2,3] the effects of power broadening will play a critical role in the design of such systems. Scientifically, the study of linewidth and dephasing mechanisms[4] in nuclear and electron magnetic resonance has been actively pursued for some 40 years. In particular, various models of host spin-flip-induced dephasing have been studied and recently extended to optical transitions.[5] In addition to the latter Monte Carlo calculation, several theoretical studies using Markovian[6–14] and non-Markovian[15] models for dephasing have appeared, all attempting to fit the DeVoe-Brewer data. As discussed by Berman[12] and Javanainen,[8] however, none of the numerical calculations presented so far consistently describe the data for $Pr^{3+}$:$LaF_3$ which includes photon echo as well as FID observations.

In this paper we extend these high-resolution FID studies to another solid, $Cr^{3+}$:$Al_2O_3$, in order to confirm the generality of the anomalous saturation behavior observed for $Pr^{3+}$:$LaF_3$ as well as to subject to theories to further comparison with experiment.

## II. THEORY

A review of various Markovian models of sudden-jump, frequency-fluctuation-induced dephasing has been given by Berman.[12] These are, under general conditions, rather complex and would require extensive numerical calculations to provide quantitative results for comparison with experiments. In this paper we restrict our theoretical discussions to two particular models, Gauss-Markov[7,9,10] (GM) and random telegraph[11] (RT) which can be numerically calculated with modest computer resources. Also, these two models have been studied previously in some detail and compared[6–14] with the first experiments with $Pr^{3+}$:$LaF_3$. Here we extend these studies to calculate the shape of the free-induction decay (FID) for the finite excitation time (200 $\mu$sec) used in the experiments.

Both models as well as the conventional OBE are described by a matrix equation

$$d\underline{\beta}/dt = \underline{M}\beta + \underline{L} \ , \tag{1}$$

where $\beta$ is the three-component Bloch vector, $\beta(1)=u$, $\beta(2)=v$, and $\beta(3)=w$ using the usual notation, and $L(1)=L(2)=0$ and $L(3)=2\gamma W_{eq}$. We assume a closed two-level system so that $2\gamma = 1/T_1$ where $T_1$ is the upper-state lifetime. We set the equilibrium value $W_{eq}=-1$. The $3\times 3$ matrix $\underline{M}$ can be written as

$$\underline{M} = -\begin{bmatrix} \gamma & 0 & 0 \\ 0 & \gamma & 0 \\ 0 & 0 & 2\gamma \end{bmatrix} + \begin{bmatrix} 0 & -\Delta & 0 \\ \Delta & 0 & \Omega \\ 0 & -\Omega & 0 \end{bmatrix} - \begin{bmatrix} \Gamma_{11} & \Gamma_{12} & \Gamma_{13} \\ \Gamma_{21} & \Gamma_{22} & \Gamma_{23} \\ 0 & 0 & 0 \end{bmatrix} , \tag{2}$$

where the first matrix accounts for lifetime damping, the second is the driving matrix, and the third is a generalized damping matrix. We consider three cases for the damping parameters.

(1) The conventional optical Bloch equations are the following:

$$\Gamma_{12}=\Gamma_{21}=\Gamma_{13}=\Gamma_{23}=0 \tag{3}$$

and

$$\Gamma_{11}=\Gamma_{22}=T_2^{-1}-\gamma \ ,$$

where $T_2$ is the dephasing time.

(2) Gaussian-Markov ($\gamma'\tau_c \ll 1$):[7,9,10]

$$\Gamma_{11}=\Gamma_{22}=\gamma'[1+(\Delta\tau_c)^2]/[1+(\Omega'\tau_c)^2] \ ,$$

$$\Gamma_{13}=\gamma'\Omega\Delta\tau_c^2/[1+(\Omega'\tau_c)^2] \ ,$$

 ©1989 The American Physical Society

$$\Gamma_{23}=-\gamma'\Omega\tau_c/[1+(\Omega'\tau_c)^2]\ , \qquad (4)$$
$$\Gamma_{12}=\Gamma_{21}=0\ ,$$

where $\gamma'=(\delta w)^2\tau_c$, $\Omega'=(\Delta^2+\Omega^2)^{1/2}$, $\Omega/2\pi$ is the Rabi frequency, $\Delta/2\pi$ is the detuning frequency, and $\delta w, \tau_c$ are parameters of the frequency fluctuation model.

(3) The third case is the random telegraph:[11]

$$\Gamma_{11}=\frac{a^2(1/\tau_c+\gamma)(1/\tau_c+2\gamma)}{P}\ ,$$
$$\Gamma_{22}=\Gamma_{11}+a^2\Omega^2/P\ ,$$
$$\Gamma_{12}=-\Gamma_{21}=-a^2\frac{\Delta(1/\tau_c+2\gamma)}{P}\ , \qquad (5)$$
$$\Gamma_{13}=\Gamma_{23}=0\ ,$$
$$P=[(1/\tau_c+\gamma)^2+\Delta^2](1/\tau_c+2\gamma)+\Omega^2(1/\tau_c+\gamma)\ ,$$

where for exponential photon-echo decay we must have $a\tau_c \ll 1$ in which case the parameter $a$ is related to the dephasing time $T_2$ by

$$T_2^{-1}=\gamma+a^2\tau_c\ . \qquad (6)$$

A matrix solution of Eq. (1) has been obtained[14] allowing numerical calculation of the Bloch vector formation during an excitation time $T$ followed by decay when the driving field is turned off. If the time variable $t=0$ at the end of the excitation, then the solution of Eq. (1) gives during the decay time

$$v(t,\Delta)=[v(T,\Delta)\cos(st)+u(T,\Delta)\sin(st)]e^{-bt}\ , \qquad (7)$$

where for the conventional OBE and GM, $b=T_2^{-1}$ and $s=\Delta$, while for RT

$$b=\gamma+\frac{a^2(1/\tau_c+\gamma)}{(1/\tau_c+\gamma)^2+\Delta^2} \qquad (8)$$

and

$$s=\Delta\left[1+\frac{a}{(1/\tau_c+\gamma)^2+\Delta^2}\right]\ . \qquad (9)$$

The amplitude $S(t)$ of the FID for a plane-wave model and infinitely wide inhomogeneous line is simply $S(t)\sim\int_0^\infty v(t,\Delta)d\Delta$. For a Gaussian-shaped beam and a Gaussian inhomogeneous width $\Delta_0$ (taken as 1 GHz in the calculations) we have

$$S(t)\sim\int_0^\infty\int_0^\infty v(t,\Delta)\exp[-(\Delta/\Delta_0)^2]\times\exp[-(r/r_0)^2]r\,dr\,d\Delta\ , \qquad (10)$$

where $r$, and $r_0$ are beam radii. Equation (10) was numerically integrated for a range of Rabi frequencies to give the theoretical time dependence of the FID decay. In general the decays are nonexponential, partly because of the finite excitation period which leads to oscillatory FID,[16] i.e., there are zero-field crossings. The theoretical linewidth, $L_t$ [half width at half maximum (HWHM)], is obtained from the expression

$$L_t=\frac{1}{2\pi}\left[\frac{1}{\tau_{\rm calc}}-\frac{1}{T_2}\right]\ , \qquad (11)$$

where $\tau_{\rm calc}$ is the $1/e$ decay time of the theoretical FID *amplitude*.

## III. EXPERIMENT

### A. Apparatus

The experimental setup is shown in Fig. 1. FID is observed following the application of a 200-$\mu$sec pulse of resonant laser light gated by an acousto-optic modulator. Following the modulator, the linearly polarized laser beam is converted to circular polarization by a quarter-wave plate and focused into the sample. This allowed selective excitation of the overlapping inhomogeneously broadened $\sigma$-polarized $R_1$ lines terminating in the ground state $^4A_2(\pm\frac{1}{2})$ levels. The transmitted light was then recollimated and directed onto an EG&G FX-100 silicon photodiode terminated by 50 $\Omega$. The FID signal was heterodyne detected at 50 MHz using the *bypassed-local-oscillator* configuration[17] shown in Fig. 1. This configuration avoids potential problems[1,18] associated with setups in which the local oscillator is transmitted through the sample. A fast rf switch (Minicircuits ZAD-1-1) was used to suppress the large transient signals which appeared on application of the light pulse. The 50-MHz rf signal was amplified by a low-noise amplifier with a 3-db bandwidth of 10 MHz (RHG Model EVT50A03DM) and then rectified by a square-law detector. The resulting FID *intensity* signal was further amplified (Princeton Model 115 preamplifier) before averaging with a Data Precision 6100 digital oscilloscope with a model 620 plug in. Finally the data was stored on a floppy disc along with the run parameters for later analysis.

The sample was a 1.6-mm-thick slab of Cochralski-grown ruby with concentration 0.0034 wt.% $Cr_2O_3$. This very dilute sample was used to avoid complications from Cr-Cr interactions[19] and necessitated signal averaging, unlike $Pr^{3+}$:$LaF_3$ (0.1% concentration) which could be measured with high signal-to-noise ratio (SNR) with a single shot. A magnetic field of $\sim$3.5 kG was applied along the $c$ axis along which the laser beam was propagated. In this work the $^4A_2(-\frac{1}{2})\rightarrow\bar{E}(-\frac{1}{2})$ transition was studied. As is well known from photon-echo modulation studies[20,21] for this transition and field, the Al spin mixing due to dipolar and exchange Cr-Al interactions is small and hence this transition is a good approximation to a two-level system. The sample was maintained at a temperature of $\sim$2 K by pumping on liquid He whose level was maintained below the sample. This procedure was found to greatly reduce the noise in the heterodyned signal caused by wave-front fluctuations generated by superfluid He. Nevertheless, wave-front fluctuations in the separate signal and local oscillator paths were troublesome leading to a fairly large scatter of the measurements as described later. From this point of view, using identical paths for the signal-local oscillator beams is advantageous.

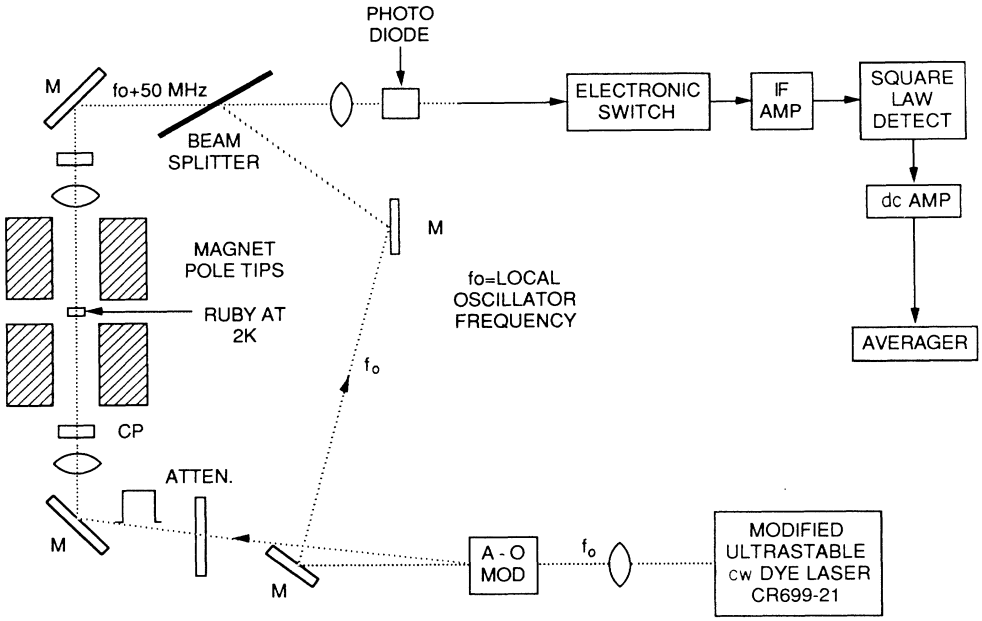


FIG. 1. Schematic of apparatus used for high-resolution free-induction-decay measurements. The bypassed-local-oscillator configuration is shown which uses an acousto-optic (AO) modulator to both pulse the laser beam and provide the local oscillator.

### B. Narrow-band dye laser

An essential requirement for high-resolution FID studies is a laser linewidth much less than the $R_1$ optical homogeneous linewidth of $\sim 20$ kHz (at fields of $\sim 4$ kG). Since the linewidth of our Coherent 699-21 ring dye laser is $\sim 1$ MHz peak to peak (P.P.) [Fig. 2(a)], modifications to the laser were necessary to reduce this width. The frequency-modulation (FM) method[22,23] of stabilization, which employs an intracavity phase modulator (AD*P), was used. The system was simultaneously locked to the Coherent low finesse Fabry-Pérot (FP) interferometer of width of $\sim 3$ GHz and an additional FP interferometer of width 1.5 MHz. The latter FP interferometer as well as another one used for linewidth measurements were wrapped in a lead-lined foam sheet and placed in hermetically sealed enclosures. The lock-up FP was a Burleigh Model CFT-100, constructed of super Invar and temperature stabilized within 0.01 °C. All components were mounted on a Newport air-mounted table. The servo electronics resembled that of Ref. 23 except that the low-frequency circuitry was not used. Instead the low-frequency error signal was fed into the first operational amplifier of the Coherent 699-21 lock-up circuit. This double-lock scheme was especially resistant to external perturbations. A measurement of the resulting laser linewidth is shown in Fig. 2(b) which gives a P.P. linewidth of $<2$ kHz for the 1-ms period of observation. For longer times ( $\sim 100$ ms), the P.P. linewidth increased to $\sim 100$ kHz. This was due to remaining vibrational effects on the observation and/or locking cavities in the frequency range $<20$ Hz. However, this longer-term jitter was presumably of no significance for the measurements in which an individual pulse preparation and FID decay sequence were completed in a time $\sim 200$ $\mu$sec.

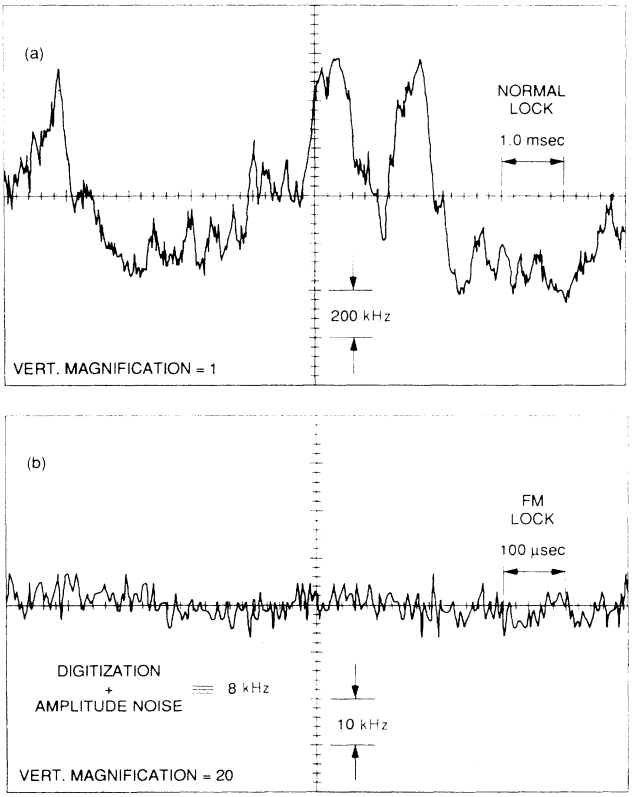


FIG. 2. Time dependence of the laser frequency obtained by measurement of the intensity transmitted through a Fabry-Pérot (FP) interferometer with the laser tuned to the 50% transmission point of the FP interferometer. A Coherent amplitude stabilizer model 307 was used to reduce amplitude fluctuations to a frequency-equivalent value of 4 kHz. (a) Normal Coherent 699-21 ring dye laser. (b) FM-stabilized Coherent 699-21 ring dye laser.

### C. Measurement and analysis methods

At the highest available dye-laser power (50–100 mW), the Rabi frequency, $\Omega/2\pi$, was measured by observation of the nutation wiggles at the leading edge of the excitation pulse. The intensity in the sample was adjusted to the desired maximum ($\sim$100 kHz) Rabi frequency by weakly focusing the beam to a diameter of 1–2 mm. These values are consistent with calculations using the Rabi equation $\Omega/2\pi = 2\mu E/h$ where[24] $\mu = 4.2\times10^{-3}D$ is the $x$ or $y$ component of the dipole moment and $E$ is the circularly polarized field. FID decays were then averaged and recorded for a number of excitation powers determined by calibrated attenuators. For each Rabi frequency, 256 traces were averaged at 20 Hz with the laser tuned to the $R_1$ line and also off the line allowing subtraction of a small background arising from rf switching transients. This subtraction as well as a regression analysis fit to a three-parameter exponential decay curve, $A + B\exp(-t/T_{\rm obs})$, were done separately on a HP9000 model 520 computer. For a measured decay time $T_{\rm obs}$ of the FID intensity, the power-broadened hole linewidth $\Delta$ (HWHM) is given by

$$\Delta = \frac{1}{2\pi}\left[\frac{1}{2T_{\rm obs}} - \frac{1}{T_2}\right],$$

where $T_2$ is the dephasing time of 15 $\mu$sec measured by photon echoes. For low excitation intensity, we found that $T_{\rm obs}\rightarrow T_2/4$ and hence $\Delta\rightarrow 1/2\pi T_2$, the normal OBE result.

### D. Results

Figure 3 shows examples of the data obtained for various Rabi frequencies. Also plotted are numerical calculations for the normal Bloch, GM and RT theories assuming $\tau_c = T_2 = 15$ $\mu$sec for GM and RT. The experimental curves decay approximately exponentially showing a slight modulation about the mean decay calculated from the nonlinear regression analysis. A summary of the linewidth dependence on Rabi frequency is given in Fig. 4. The data scatter is in part due to the problem of fitting on exponential curve to the data as well as due to the fluctuations introduced by the local-oscillator configuration as discussed earlier. Finally, we found that single-shot data agreed with those averaged at 20 Hz within 30%; however, the SNR was rather poor.

## IV. DISCUSSION AND CONCLUSION

The free-induction decay measurements of Fig. 4 indicate a hole width variation with intensity similar to that observed for $Pr^{3+}$:$LaF_3$. Both materials show a large departure from the saturation behavior predicted by the conventional Bloch equations. This saturation is, in both cases, approximately described by the GM or RT-modified OBE, with a correlation time $\tau_c = T_2$. However, such a correlation time is outside the limits of the GM theory (which requires $\tau_c \ll T_2$) or predicts nonexponential photon[8] and rotary echo decays[19] contrary to experiments.[20,21] For example, photon echoes display exponen-

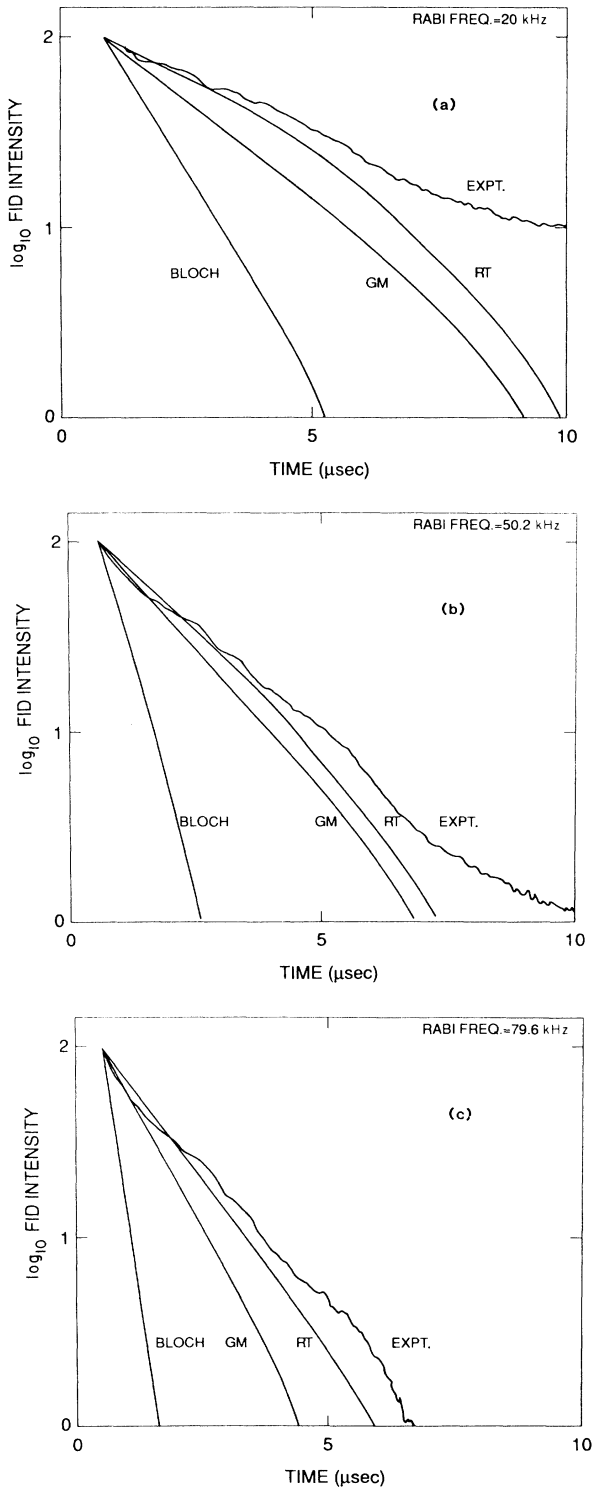


FIG. 3. Experimental and theoretical plots of free-induction-decay intensity vs time. For the Gauss-Markov (GM) and random telegraph (RT) theoretical plots, a (limiting, see text) correlation time $\tau_c = T_2 = 15$ $\mu$sec is assumed. The Bloch curve is obtained from the standard optical Bloch equations. A pulse excitation time of 200 $\mu$sec is used in the calculations. The experimental curve is the result of 256 averages. (a) Rabi frequency = 20 kHz, (b) Rabi frequency = 50.2 kHz, and (c) Rabi frequency = 79.6 kHz.

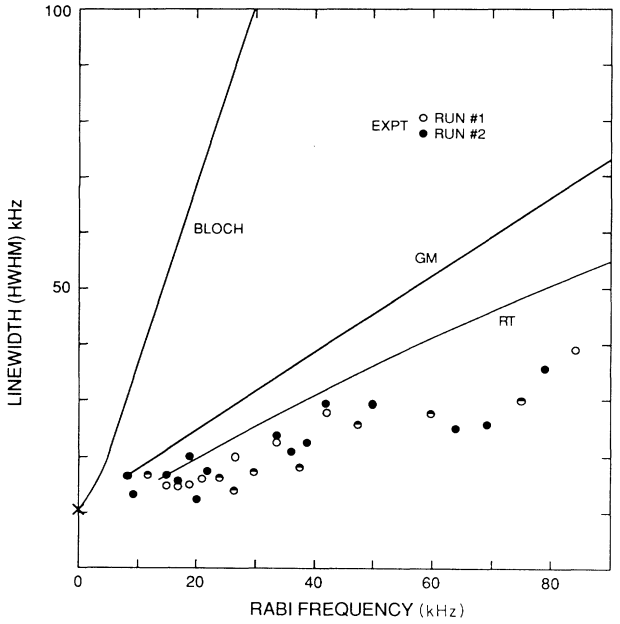


FIG. 4. Optical linewidth (HWHM) of the prepared hole vs Rabi frequency $\Omega/2\pi$ for the ${}^4A_2(-\frac{1}{2})\rightarrow\bar{E}(-\frac{1}{2})$ transition in dilute ruby (0.0034 wt.% $Cr_2O_3$) with a field of $\sim 3.5$ kG applied along the $c$ axis. Theoretical curves for the normal Bloch, Gauss-Markov (GM), and random telegraph (RT) models are also shown assuming $\tau_c = T_2 = 15$ $\mu$sec for GM and RT. The point designated by an X at zero Rabi frequency is obtained from a photon-echo measurement.

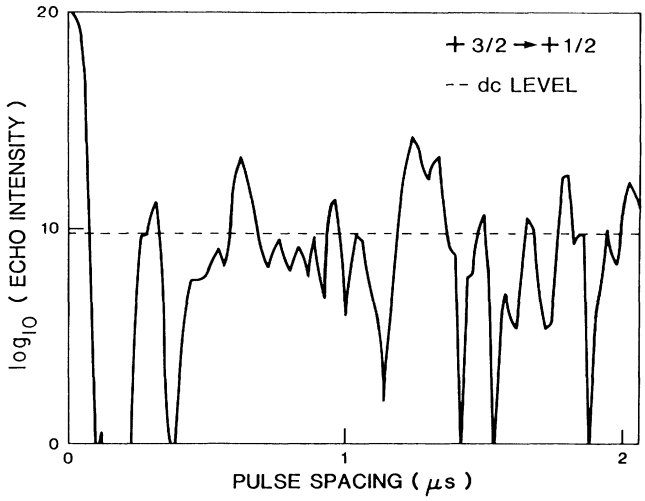


FIG. 5. Calculated photon-echo time dependence (Ref. 21) for the ${}^4A_2(+\frac{1}{2})\rightarrow\bar{E}(+\frac{1}{2})$ transition in ruby for a field of 4.0 kG applied along the $c$ axis. Dephasing time is infinite. The dc level indicates the time-independent part of the echo intensity.

tial decays over three to four orders. Our conclusion is that these particular Markovian dephasing models cannot consistently explain the FID and echo data. However, more general Markov models with various frequency-fluctuation kernels[12] remain to be numerically investigated.

Finally we speculate on whether modeling of the dephasing process by "sudden-jump," spin-flip-induced frequency shifts is a valid physical picture for solids. Alternative pictures[4,25,26] view dephasing as a modulation or quantum-interference process which, because of the complexity of the large number of interactions, never results in return of an initially induced coherence. An indication of this kind of behavior has appeared in earlier[21] calculations of echo modulation for the ${}^4A_2(+\frac{3}{2})\rightarrow\bar{E}(+\frac{1}{2})$ transition in ruby. We reproduce the result of this calculation in Fig. 5. Generally echo modulation due to hyperfine (or superhyperfine) interactions is described by a dc or time-independent term[21] and a time-dependent one which contains sum and difference frequencies of the ground- and excited-state hyperfine frequencies. The time-dependent terms describe a modulation of the echo around the dc level. Because of the large spin mixing for this transition, the dc term in Fig. 5 is some ten orders of magnitude below the zero-time-echo value. While this appears to lead to dephasing of the echo in the first $\sim 100$ nsec, it should be stressed that this is a deterministic quantum interference effect unrelated to stochastic dephasing. The calculation of Fig. 5 does not include any stochastic mechanisms. The Hamiltonian for the system is written as

$$H_0 = H_{\mathrm{Cr}} + \sum_{\mathrm{Al}} (H_{\mathrm{Al}} + H_{\mathrm{Cr-Al}} + H_{\mathrm{Al-Al}}) ,$$

where the Cr-Al interaction arises from exchange and dipolar effects and the Al-Al interaction is dipolar. In echo modulation calculations, the $H_{\mathrm{Al-Al}}$ terms are omitted which permits an analytical solution of the problem. Of course it is these terms which give rise to the host spin flipping. In the quantum interference picture, inclusion of these terms would presumably push the dc echo term to zero. Alternately, we could imagine that the dc term would undergo an exponential decay which is the *ad hoc* procedure used[21] to compare theoretical and experimental modulated echo decays.

In conclusion, we have found that the Gauss-Markov or random-telegraph modifications of the optical Bloch equations do not consistently describe free-induction and echo-decay measurements with a single correlation time for the assumed stochastic frequency fluctuations. It is suggested that a nonstochastic model[26] involving chaotic quantum-interference effects may be useful to study.

## ACKNOWLEDGMENTS

Helpful discussions with Professor T. Hashi and Professor T. Endo are gratefully acknowledged as is the expert technical assistance of J. Froemel.

*Permanent address: Shiga University, Otsu 520, Japan.
[1]R. G. DeVoe and R. G. Brewer, Phys. Rev. Lett. **50**, 1269 (1983).
[2]A. Szabo, U.S. Patent No. 3 896 420 (22 July 1975); G. Castro, D. Haarer, R. M. Macfarlane, and H. P. Trommsdorf, U.S. Patent No. 4 101 976 (18 July 1978).
[3]W. E. Moerner, J. Mol. Electron. **1**, 55 (1985), and references therein.
[4]W. B. Mims, in *Electron Paramagnetic Resonance,* edited by S. Geschwind (Plenum, New York, 1972), pp. 263–351.
[5]R. G. DeVoe, A. Wokaun, S. C. Rand, and R. G. Brewer, Phys. Rev. B **23**, 3125 (1981).
[6]E. Hanamura, J. Phys. Soc. Jpn. **52**, 2258 (1983).
[7]M. Yamanoi and J. H. Eberly, Phys. Rev. Lett. **52**, 1353 (1984); J. Opt. Soc. Am B **1**, 751 (1984).
[8]J. Javanainen, Opt. Commun. **50**, 26 (1184).
[9]A. Schenzle, M. Mitsunaga, R. G. DeVoe, and R. G. Brewer, Phys. Rev. A **30**, 325 (1984).
[10]P. R. Berman and R. G. Brewer, Phys. Rev. A **32**, 2784 (1985).
[11]K. Wodkiewicz and J. H. Eberly, Phys. Rev. A **32**, 992 (1985).
[12]P. R. Berman, J. Opt. Soc. Am B **3**, 564 (1986); **3**, 572 (1986).
[13]M. Yamanoi and J. H. Eberly, Phys. Rev. A **34**, 1609 (1986).
[14]A. Szabo and T. Muramoto, Phys. Rev. A **37**, 4040 (1988).
[15]P. A. Apansevich, S. Ya. Kilin, A. P. Nizovtsev, and N. S. Onishchenko, Opt. Commun. **52**, 279 (1984).
[16]A. Schenzle, N. C. Wong, and R. G. Brewer, Phys. Rev. A **21**, 887 (1980).
[17]P. E. Jessop and A. Szabo, Phys. Rev. B **26**, 420 (1982).
[18]R. M. MacFarlane, R. M. Shelby, and R. L. Shoemaker, Phys. Rev. Lett. **43**, 1726 (1979).
[19]T. Muramoto and A. Szabo, Phys. Rev. A **38**, 5928 (1988).
[20]S. Meth, Ph.D. dissertation, Columbia University, New York, 1977.
[21]A. Szabo, J. Opt. Soc. Am B **3**, 514 (1986).
[22]R. W. P. Drever, J. L. Hall, F. V. Kowalski, J. Hough, G. M. Ford, A. J. Munley, and H. Ward, Appl. Phys. B **31**, 91 (1983).
[23]J. Helmcke, S. A. Lee, and J. L. Hall, Appl. Opt. **21**, 1686 (1982).
[24]Calculated from the data in P. E. Jessop and A. Szabo, in *Laser Spectroscopy V,* edited by A. R. W. McKellar, T. Oka, and B. P. Stoicheff (Springer-Verlag, Berlin, 1981), p. 408. An earlier estimate gave $\mu=4.8\times10^{-3}D$ for the ${}^4A_2(\pm\frac{1}{2})\rightarrow\bar{E}(\pm\frac{1}{2})$ $\sigma$ transition. See S. L. McCall and E. L. Hahn, Phys. Rev. **183**, 457 (1969).
[25]J. P. Hurrel and E. R. Davies, Solid State Commun. **9**, 461 (1961).
[26]T. Endo, J. Phys. Soc. Jpn. **56**, 1684 (1987).